ACS APPLIED BIO MATERIALS Cite This: ACS Appl. Bio Mater. XXXX, XXX, XXX−XXX

Article

www.acsabm.org

Supramolecular Hydrogels with Properties Tunable by Calcium Ions: A Bio-Inspired Chemical System

Demetra Giuri,[†] Lara Jurković,[‡] Simona Fermani,[†] Damir Kralj,[‡] Giuseppe Falini,*[,†] and Claudia Tomasini*[,†]

[†]Dipartimento di Chimica "Giacomo Ciamician", Alma Mater Studiorum - Università di Bologna, via Selmi 2, 40126 Bologna, Italy

[‡]Rudjer Boskovic Institute, Bijenicka 54, 10000 Zagreb, Croatia

Supporting Information

ABSTRACT: Boc-L-DOPA(OBn)$_2$-OH is a simple synthetic molecule that promotes hydrogelation through electrostatic and $\pi-\pi$ stacking interactions. Hydrogelation can occur in alkaline conditions by the use of triggers. Four hydrogels were prepared varying the base, NaOH or Na_2CO_3, and the trigger, GdL or $CaCl_2$. When the hydrogel formed in the presence of Na_2CO_3 and $CaCl_2$, the concomitant production of $CaCO_3$ crystals occurred, generating an organic/inorganic composite material. It was observed that the hydrogel once self-assembled preserved its status even if the trigger, the calcium ions, was removed. The viscoelastic behavior of the hydrogels was analyzed through rheological experiments, which showed a solid-like behavior of the hydrogels. The corresponding xerogels were analyzed mainly by scanning electron microscopy (SEM) and synchrotron X-ray diffraction analysis (XRD). They showed differences in structure, morphology, and fiber organization according to their source. This research presents a hydrogel system that can be applied as a soft biomaterial for tissue engineering, cosmetics, food, and environmental science. Moreover, it represents a model for biomineralization studies in which the hydrogel structure can act as an analogue of the insoluble matrix that confines the calcification site, provides Ca^{2+}, and preserves its structure.

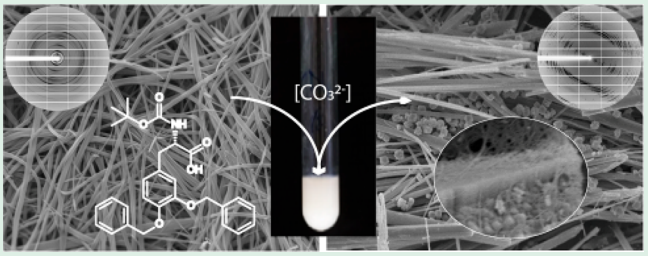

KEYWORDS: *hydrogels, self-assembled fibrillary network, composite materials, calcium carbonate, biomineralization*

INTRODUCTION

The preparation and application of self-assembled fibrillar network (SAFiN) hydrogels and organogels is a topic that recently received great attention due to the wide applicability of this class of soft materials in the fields of tissue engineering, cosmetics, food, and environmental science.[1−6] They were also used in recent material-processing techniques, such as three-dimensional[7] and four-dimensional printing.[8]

The principal constituents of SAFiN gels are low-molecular-weight gelators (LMWGs),[9−12] small compounds that have attracted a large amount of interest for their easily attainable and modifiable chemical structures that produce materials with different properties. Fluorenyl-9-methoxycarbonyl (Fmoc) amino acid derivatives[13−15] are one of the most popular classes of LMWGs, but amino acids, small peptides, or glycolipids[16−21] are also largely explored. Usually, LMWGs have a molecular weight not exceeding 1000 Da, are often chiral with a specific stereochemistry,[22] and can self-assemble thanks to weak interactions such as hydrogen bonds, $\pi-\pi$ stacking, and van der Waals forces.[23−25] Gelation starts with the dissolution of the LMWG into a solvent, is generally driven by weak interactions, and can be triggered by numerous stimuli such as temperature,[26] pH,[27] or inorganic salt.[28,29]

The hydrogel formation usually takes place within a few hours through the slow formation of fibers that entrap the solvent. The gels may be constituted of water or an organic solvent, in which a wide variety of materials can be dissolved or suspended and finally trapped into the gel structure, such as graphene,[30−33] cells,[15,34,35] and catalysts.[36,37] After the hydrogel formation, several processes may take place in the confined space of the gel, producing results that are different from that observed in solution.

In this context, hydrogels also have relevance in biomineralization, which is the process by which organisms deposit in a controlled way mineral phases producing composite inorganic/organic biominerals, such as bones, teeth, and mollusk shells.[38−40] The biominerals have properties optimized for the specific function they have to carry out, which so far are impossible to reproduce by laboratory activities. The experimentally proved dogma of biomineralization is that the deposition of the mineral phase occurs in a highly viscous or gel environment.[38,41] This observation has stimulated the study of the formation of biominerals in hydrogels, using both

Received: September 12, 2019
Accepted: November 18, 2019
Published: November 18, 2019

Downloaded via UNIV BOLOGNA on November 29, 2019 at 13:58:46 (UTC).
See https://pubs.acs.org/sharingguidelines for options on how to legitimately share published articles.

© XXXX American Chemical Society

DOI: 10.1021/acsabm.9b00828
ACS Appl. Bio Mater. XXXX, XXX, XXX−XXX

synthetic and natural (macro)molecular gelators. Examples of natural physical gelators are biopolymers of polysaccharides such as agarose, pectin, and cellulose, as well as proteins such as collagen, gelatin, and silk fibroin.[42] Other natural low molecular weight molecules can also form gels, like glycosyl-nucleoside lipids.[43] Calcium carbonate has been one of the most studied minerals because it is widespread among organisms and represents a relatively simple chemical system to investigate *in vitro*.[44] Examples of hydrogels in biological as well as synthetic, bioinspired systems are discussed in Asenath-Smith et al.[45] and report the physical versus chemical effects of a broad range of hydrogel matrices and their role in directing polymorph selectivity and morphological control in the calcium carbonate system. Indeed, either the function of the gel has been to physically control the diffusion process of precipitating ions or the gelator molecule's functional groups chemically interact with the growing crystals of the mineral phase. In recent research, a gel formed in the presence of calcium ions was used as a source of calcium ions for calcification. However, the gel structure was typically lost during the calcification process.[46] Examples of hydrogels that form a framework in the presence of calcium ions that provide the calcium ions for crystallization and preserve their framework structure are absent in the literature. Such a system may be of great relevance in biomineralization since in many organisms the mineralization process occurs in a gelling confined environment rich in calcium ions in which carbonate ions diffuse.[38,47]

Here we report the results obtained by the formation of hydrogels based on (*S*)-*N*-*tert*-butoxycarbonyl-3,4-bis-(benzyloxy)-phenylalanine [Boc-L-DOPA(OBn)$_2$-OH], using different triggers, like pH variation or addition of calcium ions. The hydrogels' mechanical properties strongly depend on the hydrogel composition and gelation technique. The hydrogel obtained in the presence of calcium ions was then used as a model system for the bionspired precipitation of calcium carbonate.

EXPERIMENTAL SECTION

Materials. All chemicals and solvents were purchased from Sigma-Aldrich, VWR, Iris Biotech, or TCI and used as received. Milli-Q water (Millipore, resistivity = 18.2 mΩ cm) was used throughout. All reactions were carried out in dried glassware. All compounds were dried in vacuo, and all the sample preparations were performed in a nitrogen atmosphere. NMR spectra were recorded with a Varian Inova 400 spectrometer at 400 MHz (^{1}H NMR).

Synthesis of Boc-L-Dopa(OBn)$_2$-OH. Boc-L-Dopa(OBn)$_2$-OH was synthesized following a multistep procedure in solution as reported in the literature.[48,49]

Conditions for Gel Formation. The control sample (**1**) was prepared by adding Milli-Q water (0.97 mL) and aqueous 1 M NaOH (1.3 equiv) to a test tube (8 mm of diameter) containing 10 mg of the compound, in order to produce a final concentration of the gelator of 1% w/w. The mixture was stirred and sonicated in turn for about 30 min until the complete dissolution of the sample. Then glucono-δ-lactone (GdL 1.4 equiv) was added to the mixture. After a rapid mixing and complete dissolution of GdL, the sample was allowed to stand quiescently until gel formation, which occurs during several hours.

Sample **2** was prepared by adding Milli-Q water (0.76 mL) and aqueous 1 M NaOH (1.3 equiv) to a test tube (8 mm of diameter) containing 10 mg of the compound to produce a final concentration of the gelator of 1% w/w. The mixture was stirred and sonicated in turn for about 30 min, until the complete dissolution of the sample. Then a 0.1 M aqueous $CaCl_2$ (1 equiv) was added to the mixture. After a rapid and complete dissolution of $CaCl_2$, the sample was allowed to stand quiescently before further studies, even if the formation of gel occurs immediately.

Samples **3** and **4** were prepared following the same procedure as for sample **2**, but instead of NaOH, Na_2CO_3 was used. In sample **4**, 1 equiv of Na_2CO_3 and 1 equiv of $CaCl_2$ were added, while in sample **4**, 2.5 and 5 equiv, respectively, were added (see Table 1).

Table 1. Reagents, Conditions, and Final pH for Hydrogel Formation Using Gelator A in 1 wt. % Concentration

sample	gelator (mg)	equiv of NaOH (1 M)	equiv of Na_2CO_3 (0.1 M)	equiv of GdL	equiv of $CaCl_2$ (0.1 M)	final pH
1	10	1.3	-	1.4	-	5.5
2	10	1.3	-	-	1	8
3	10	-	1	-	1	6
4	10	-	2.5	-	5	6.5

Rheology. Rheological measurements were performed on an Anton Paar Rheometer MCR 102 using a parallel plate configuration (25 mm diameter). The experiments were performed at a constant temperature of 23 °C, controlled by the integrated Peltier system. All analyses were performed with a fixed gap value of 0.5 mm on the respective gel samples, prepared the day before the analysis, and left overnight at a controlled temperature of 20 °C to complete the gelation process (around 20 h). Oscillatory amplitude sweep experiments (γ: 0.01−100%) were carried out to determine the linear viscoelastic (LVE) range at a fixed frequency of 1 rad s^{-1}. Once the LVE of each hydrogel was established, frequency sweep tests were performed (ω: 0.1−100 rad s^{-1}) at a constant strain within the LVE region of each sample (γ = 0.04%). Step strain experiments were performed on hydrogels to analyze the thixotropic behavior of the material. The sample was subjected to consecutive deformation and recovery steps. The recovery step was performed by keeping the sample at a constant strain γ = 0.04%, i.e., within the LVE region, for a period of 400 s. The deformation step was performed by applying to the gel a constant strain of γ = 100%, i.e., above the LVE region of the sample for a period of 300 s. The cycles were performed three times at a fixed frequency of ω = 10 rad s^{-1}.

Sample Preparation for X-ray Diffraction (XRD) and Scanning Electron Microscopy (SEM) Analysis. Two procedures were used for the preparation of the xerogels. (a) The hydrogels were directly oven-dried at 100 °C for 2 h without any washing process. (b) Each hydrogel (1 mL) was washed twice, with Milli-Q water (2 mL) followed by ethanol (2 mL). In both cases, after the solvent addition, the test tube containing the sample was stirred with a Vortex (1 min) and centrifuged (5 min−5000 rpm) and then the supernatant was removed. The solid residue was oven-dried at 100 °C for 2 h.

EDTA Treatment. After gelation, hydrogel **2** (1 mL) was placed in a vial with 6 mL of a 0.05 M Na_2EDTA solution and gently stirred for 5 h. Then, the solution was removed, and the sample was used for rheological analyses (**2E**). Before SEM and XRD analysis, the samples were washed according to the procedure reported above.

EDTA-$CaCl_2$ Treatment. After gelation, hydrogel **2** (1 mL) was placed in a vial with 6 mL of a 0.05 M Na_2EDTA solution and gently stirred for 5 h. Then, the solution was replaced with 6 mL of a 0.1 M $CaCl_2$ solution. The solution was removed after 5 h, and the sample was used for rheological analyses (**2Ca**). Before SEM and XRD analysis, the samples were washed according to the procedure reported above.

Scanning Electron Microscopy. For the SEM imaging, the uncoated samples were observed with a Phenom G2 Pure using an energy of 3 kV. Gold-coated (2 nm) samples were observed using a Hitachi SEM 6400 operating at 15 kV.

X-ray Fiber Diffraction. X-ray diffraction images were collected at the XRD1 beamline, Elettra, Trieste, Italy and at the beamline ID23-1, ESRF, Grenoble, France. Each frame was collected at the

DOI: 10.1021/acsabm.9b00828
ACS Appl. Bio Mater. XXXX, XXX, XXX−XXX

peak wavelength (0.9765 Å) using an exposure of 60 s. The XRD diagrams were analyzed using Fit2D software.[50]

Number of Experiments. All the experiments for the preparation of the hydrogel **1**, **2**, **3**, **4**, **2-E**, and **2-Ca** were repeated at least three time. The preparation of the xerogels was performed using two experimental procedures that were also repeated at least three times for each sample. The scanning electron microscopy observations were performed on at the least three independent samples for each preparation. The rheological and diffractometric measurements were performed on one sample.

RESULTS AND DISCUSSION

Recently, we investigated the formation of SAFiN hydrogels and organogels, using LMWGs containing either protected amino acids or the pseudoproline (4*R*,5*S*)-4-methyl-5-carboxyl-oxazolidin-2-one (D-Oxd), and we could demonstrate that they have an essential role in the design of efficient gelators.[51,52] We also tested the gelation ability of an L-DOPA derivative, which forms strong supramolecular hydrogels and organogels.[53,54] For our continuous effort to find some new gelators able to form stable hydrogels useful for different applications, now we show the results obtained using Boc-L-DOPA(OBn)$_2$-OH (**A**) as the hydrogelator (Figure 1). This compound displays two additional benzyl esters in the chemical structure that should improve its gelation efficiency through additional $\pi-\pi$ stacking interactions.

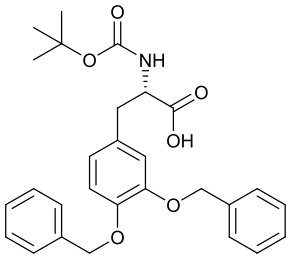

Figure 1. Chemical structure of Boc-L-DOPA(OBn)$_2$-OH **A**.

Hydrogel Formation and Calcification Process. The synthesis of gelator **A** started from unprotected and commercially available L-DOPA, which was transformed into Boc-L-DOPA(OBn)$_2$-OH (Figure 1) through four steps (Scheme S1 in the Supporting Information) on a multigram scale with excellent yields, following a literature procedure.[48,49] The simplicity in the preparation of this compound is, therefore, an important point in favor of the application of this new molecule for the formation of supramolecular materials.

The preparation of the hydrogels followed a general procedure based on the gelator dissolution in an aqueous NaOH solution (for details, see Table 1), by stirring and sonication for about 15 min, followed by the addition of the trigger (GdL or $CaCl_2$).[23,51,55−58] After several attempts, we found that the optimal gelator concentration is 1% w/w. Moreover, before choosing the optimal Na_2CO_3 and $CaCl_2$ concentrations used for samples **2**, **3**, and **4**, we tested other concentrations that resulted to be low (10 mM) to detect the calcite formation or too high (100 mM) to obtain a strong hydrogel. Samples **1** and **2** were prepared following this protocol but changing the triggers (GdL and $CaCl_2$, respectively). For the preparation of samples **3** and **4**, NaOH was replaced by Na_2CO_3 which is the source of carbonate ions to induce the formation of $CaCO_3$ crystals, after the addition of the trigger $CaCl_2$. Following this procedure, the formation of the gel takes place with the formation of $CaCO_3$ crystals.

In all the cases, a rapid gel formation was detected, soon after the addition of the trigger, even in the case of the GdL, which usually requires prolonged times to form the network.[59] All gels appear homogeneous and opaque (Figure 2). The final

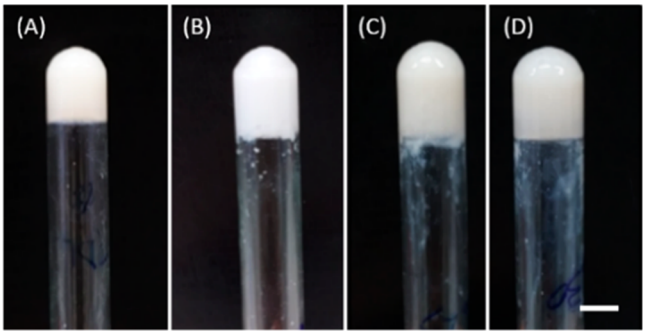

Figure 2. Photographs of the hydrogels prepared using gelator **A** in 1 wt. %. From the left: **1** (A), **2** (B), **3** (C), and **4** (D). Scale bar: 5 mm.

pH of the gel was affected by the chemical processes occurring in it. When the environment was alkaline after the addition of NaOH and the trigger was $CaCl_2$, the final pH was 8. Since the starting concentration of $[OH^-]$ was 1 M, this final value suggests that a relevant part of the OH^- groups was involved in the salification of the gelator. When Na_2CO_3 was used instead of NaOH, the drop of pH was higher (samples **3** and **4** of Table 1), and this occurred because the Na_2CO_3 was consumed not only by the salification process but also by the formation of $CaCO_3$.

Hydrogel Characterization. *Rheological Analysis.* The viscoelastic behavior of the hydrogels in terms of storage (G') and loss (G'') moduli was analyzed using rheological experiments. The LVE (linear viscoelastic) range was evaluated through shear strain experiments, with a constant frequency ω = 1 rad s^{-1} (Figure S1). All the hydrogels prepared are characterized by G' approximately an order of magnitude higher than G'' (except samples 30 that are highly calcified), indicating their solid-like behavior.[23,60] Frequency sweep experiments (Figure 3), performed by applying a constant shear strain within the LVE region of each sample, confirmed the "solid-like" behavior for all the hydrogels and showed that both the G' and G'' were almost independent from frequency in the range from 0.1 to 100 rad s^{-1}, with G' always greater than G'' (see Table 2).

Additionally, the system's ability to recover the gel status after a strong stress that induces transformation into sol (thixotropy) was checked. Thixotropy[61−64] is often related to self-healing properties[16,65−68] and may be defined as the ability to autonomously reconstruct the bonding interactions after damage. To check if the hydrogels are endowed with these properties, four samples were subjected to a strain value within the LVE region (characterized by G' values greater than G''), and multiple cycles of two steps were applied to the respective hydrogels (Figure 4). When the applied strain was increased above the crossover point, the sample behavior switched from gel-like to sol-like, with G'' values greater than G'. Finally, the samples rested at fixed strain within the LVE range to check the recovery of the gel-like status. Samples **1**, **3**, and **4** showed good thixotropic behavior, as they promptly recovered their properties after each cycle. In contrast, hydrogel **2** recovered a

DOI: 10.1021/acsabm.9b00828
ACS Appl. Bio Mater. XXXX, XXX, XXX−XXX

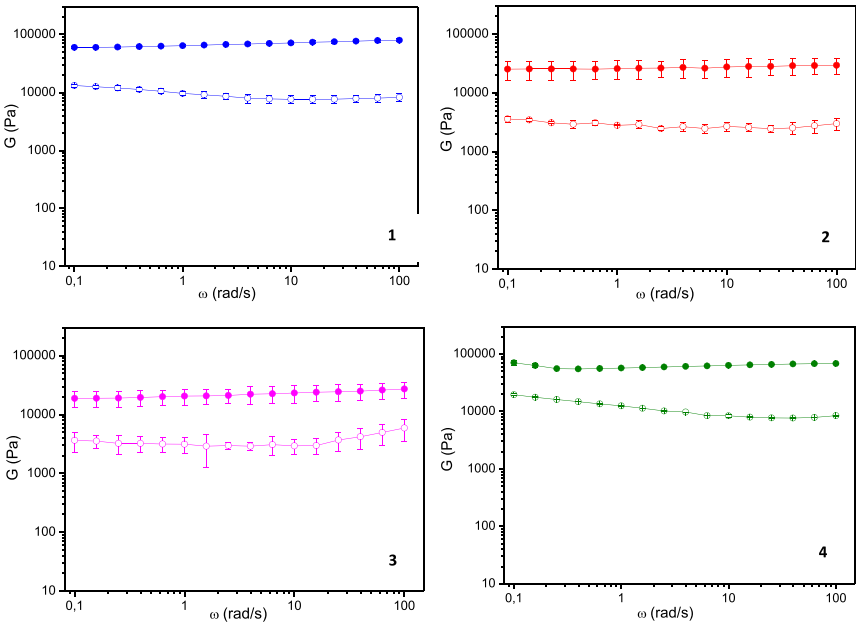

Figure 3. Frequency sweep experiments (constant $\gamma = 0.04\%$) performed on the 1 wt.% hydrogels. The analyses were performed in duplicate on the hydrogels about 20 hours after the gelation has begun.

Table 2. G' and G'' Mean Moduli and Standard Deviation from Frequency Sweep Experiments ($\gamma = 0.04\%$, $\omega = 1$ rad/s)

sample	G' (KPa)	G'' (KPa)
1	64.181 ± 2.761	9.648 ± 0.884
2	25.800 ± 9.051	2.790 ± 0.042
3	20.650 ± 6.435	3.140 ± 0.990
4	56.738 ± 0.735	12.507 ± 0.111

gel-like status after the first cycle, although the G' value is significantly reduced (21 000 Pa → 360 Pa). After the second cycle, the hydrogel recovered again a gel-like behavior with a G' value of about 400 Pa.

Reversibility of Calcium Ion Uptake by the Hydrogel. To check if Ca^{2+} was pivotal for hydrogel formation, a sample of hydrogel **2** was immersed in a disodium ethylenediaminetetraacetate dihydrate (EDTA) solution under gentle stirring for 5 h, in order to replace Ca^{2+} with H^+ in the hydrogel structure

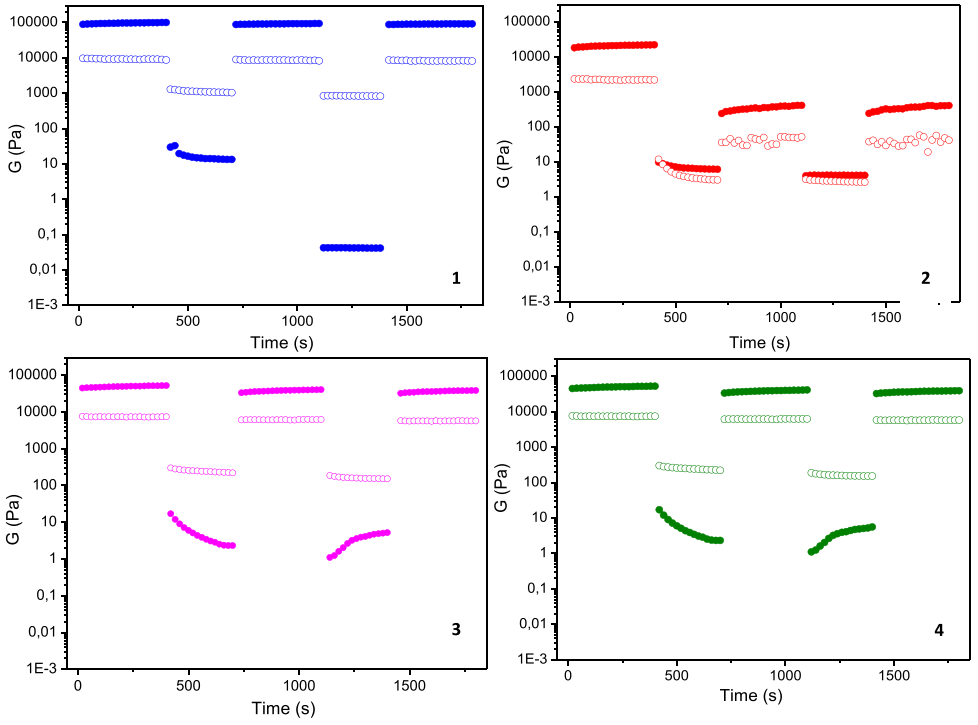

Figure 4. Values of storage moduli G' (solid circles) and loss moduli G'' (empty circles) recorded during step strain experiments performed on the hydrogel samples **1**, **2**, **3** and **4**.

DOI: 10.1021/acsabm.9b00828
ACS Appl. Bio Mater. XXXX, XXX, XXX−XXX

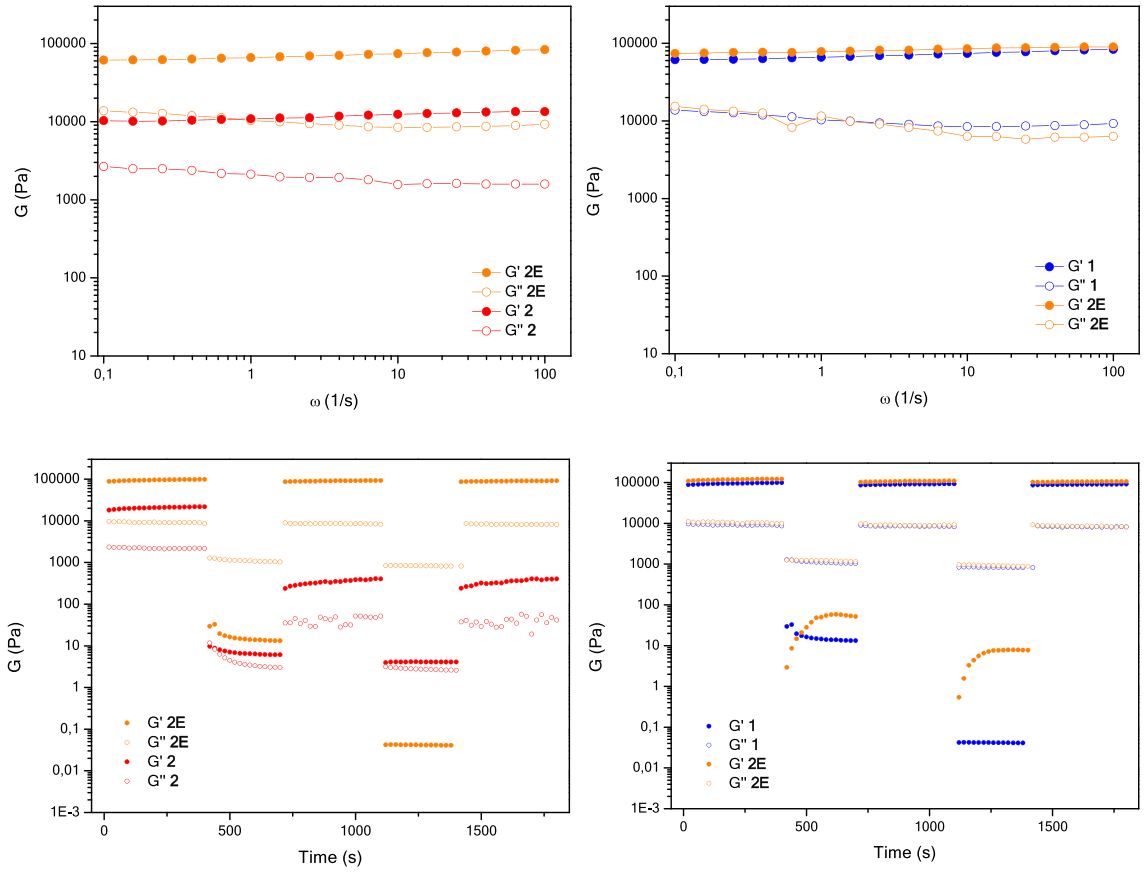

Figure 5. (Top) Frequency sweep experiments (constant γ = 0.04%) performed on the 1 wt % hydrogels. The results obtained for **2E** were compared with **2** (left) and **1** (right). (Bottom) Values of storage moduli G' (solid circles) and loss moduli G'' (empty circles) recorded during step strain experiments performed on the hydrogels. The results obtained for **2E** were compared with **2** (left) and **1** (right).

(see Experimental Section for details). After the treatment, the sample was Ca^{2+} free, as verified by the energy-dispersive X-ray spectroscopy (EDX) spectrum of a fragment of the dry samples (later named as **xero-2**) in which no signal for calcium was observed (Figure S5).

The mechanical properties of the sample treated with EDTA (**2E**) were analyzed with the rheometer and compared with those of sample **2** (Figure 5). We found that sample **2E** is much stronger than sample **2**, showing properties similar to those of sample **1**. When hydrogel **2E** was resuspended in a $CaCl_2$ solution for 5 h (**2Ca**), no variation in its aspect neither on its mechanical properties was observed (Figure S4). These outcomes suggest that a modification of the supramolecular fiber organization occurs upon Ca^{2+} removal, and this modification is not reversible by re-adding calcium ions. Despite this, the corresponding dry samples (later named as **xero-2Ca**) showed the presence of about 1 atom % content of calcium, as illustrated by the EDX spectrum reported in Figure S5.

These outcomes suggest that a modification of the supramolecular fiber organization occurs upon Ca Ca^{2+} removal, and this modification is not reversible by re-adding calcium ions. Despite this, the corresponding dry samples (later named as **xero-2Ca**) showed the presence of about 1 atom % content of calcium, as illustrated by the EDX spectrum reported in Figure S5.

A possible reason for this behavior can be found in the pH change during the treatment. After the removal of calcium with EDTA from hydrogel **2** to form **2E**, the pH decreased from 8 to 4 and remained unchanged when sample **2E** was resuspended in the calcium solution.

Xerogel Characterization. To perform the SEM and synchrotron XRD analyses, the hydrogels **1**, **2**, **3**, **4**, **2E**, and **2Ca** were converted into xerogels by solvent removal in an oven. The dried samples were washed with ethanol, dried again, and named **xero-1**, **xero-2**, **xero-3**, **xero-4**, **xero-2E**, and **xero-2Ca**. Some samples of hydrogels **3** and **4** were prepared with a modified procedure, based on washing with water and ethanol followed by solvent removal in the oven, thus forming the modified xerogels **xero-3#** and **xero-4#**. This procedure was envisaged to remove unreacted ions and molecules and change the hydrogel chemical environment before drying.

The SEM images of the samples **xero-1**, **xero-2**, **xero-3**, and **xero-4** are reported in Figure 6. **Xero-1** and **xero-2** show differences in morphology and fiber organization. Indeed, in the sample **xero-1** the fibers, around 25 nm in diameter, are partially embedded in a matrix that prevents an accurate determination of the average diameter. In the sample **xero-2**, the fibrous structure is well evident, and the fibers form a network in which they are strongly entangled, thanks also to the branching that appears in some fibers. Both **xero-3** and **xero-4** show a fibrous structure, where entrapped calcium carbonate crystals are present. Both composites show a high embedding of the crystals inside the fibrous network. The fibers entrap the crystals almost completely and also penetrate inside them, thus forming an organic−inorganic composite

DOI: 10.1021/acsabm.9b00828
ACS Appl. Bio Mater. XXXX, XXX, XXX−XXX

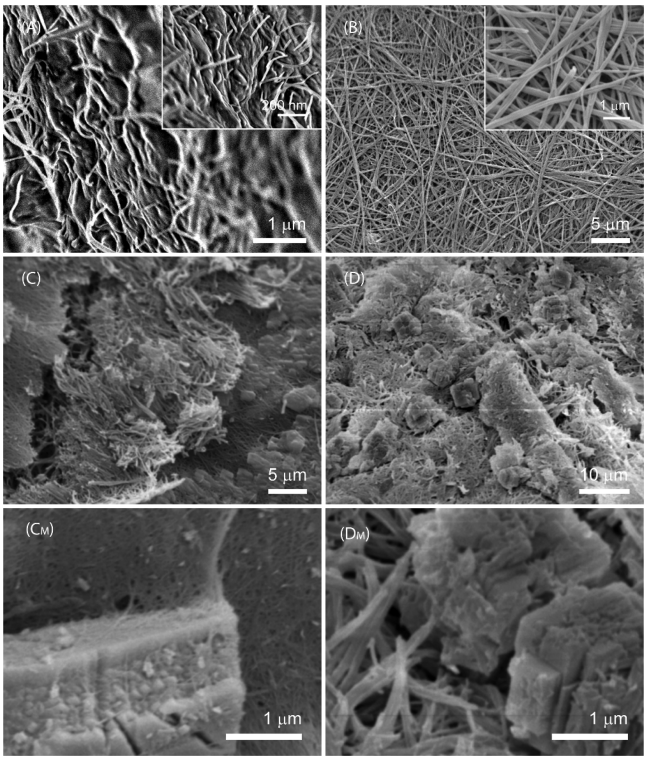

Figure 6. SEM images of the xerogel samples **xero-1** (A), **xero-2** (B), **xero-3** (C, C_M), and **xero-4** (D, D_M). The insets in (A) and (B) illustrate a high-magnification image for **xero-1** and **xero-2**. The images (C_M) and (D_M) illustrate the composite nature of the calcite crystals from **xero-3** and **xero-4** that entrap gelator fibers. Each image is representative of the entire sample (additional images are reported in Figure S9).

material (Figures 6E, 6F, and S9). The amount of crystals observed in samples **xero-3** is lower than that in samples **xero-4**, as expected since in the starting hydrogel chemical system the concentrations of calcium and carbonate ions were lower.

The SEM images of the xerogels **xero-2E** and **xero-2Ca** are reported in Figure 7 (left). They show that the sample **xero-2E** has the same fiber organization observed in the sample **xero-2**. The fibers have an almost constant diameter and are strongly entagled. The sample **xero-2Ca** is heterogeneuos and both fibers, like those observed in the sample **xero-2**, and less defined segments, like those observed in the sample **xero-3** (or **xero-4**), may be observed.

The fiber diameter distribution observed by the SEM images for samples **xero-2**, **xero-2E**, and **xero-2Ca** ($n \geq 50$) was analyzed through a box plot.[69] The box plots are shown in Figure 7 (right) and reveal a different diameter of the fibers obtained in the diverse conditions. They underline that when the calcium ions are involved in the formation of the hydrogels the fibers are thin. Alternately, when the calcium ions are removed by the hydrogel fibers by the interaction with EDTA, a fiber aggregation process occurs, which is preserved in the xerogel.

The structure of the xerogels was investigated by synchrotron X-ray diffraction. The corresponding X-ray powder diffraction patterns, which were obtained by integration of the intensities along the 2Θ angle, are reported in Figures 8 and 9. These data show that all xerogel samples were crystalline and with different structures, according to their synthesis, or their postsynthesis treatment. The xerogels **xero-1**, **xero-2**, **xero-3**, and **xero-4** show intense low-angle diffraction peaks at 2.99 and 1.74 nm; in addition, intense diffraction peaks at 0.51, 0.46, and 0.34 nm are also observed (Figure 8). The relative intensity of these peaks is different among the samples, and this observation can be due to the preferential orientation effect. Other diffraction peaks were also observed at 1.46, 0.99, 0.92, 0.67, and 0.61 nm that were common among the samples **xero-2**, **xero-3**, and **xero-4**. The sample **xero-1** shows diffraction peaks at 1.34 and 0.83 nm that are absent in the other samples, which are formed in the presence of Ca^{2+}, suggesting that in the presence of GdL the Boc-L-DOPA$(OBn)_2$-OH assembly occurs differently or with a diverse packing.

Different structures from those described before were observed in samples **xero-2E** and **xero-2Ca** (Figure 9). They were obtained by EDTA decalcification of sample **2** and subsequent incubation in $CaCl_2$, respectively. Their diffraction patterns showed several diffraction peaks having the same periodicities but with different relative intensities. Most of these diffraction peaks were at different periodicities from those observed in the samples **xero-1**, obtained in the absence

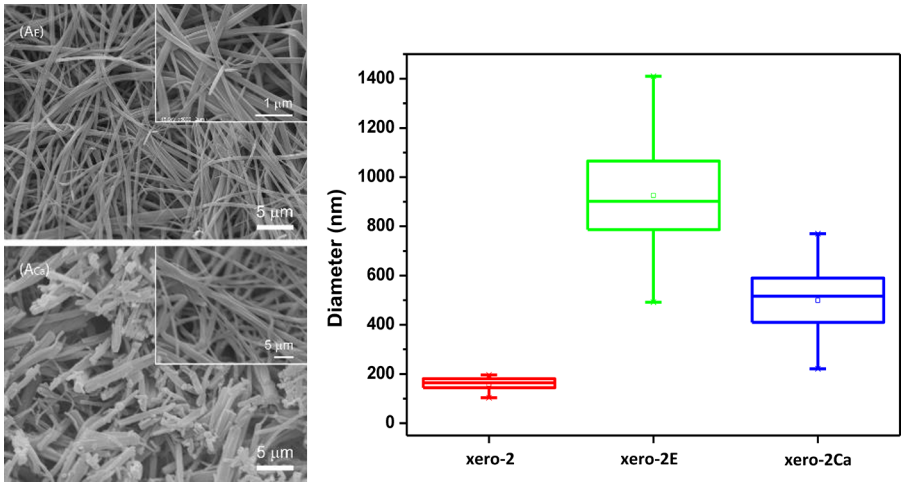

Figure 7. (left) SEM images of the xerogel samples **xero-2E** (AE) and **xero-2Ca** (ACa). (right) Box plot distribution of the fiber diameters measured in the xerogel obtained from the samples **xero-2**, **xero-2E** and **xero-2Ca**.

DOI: 10.1021/acsabm.9b00828
ACS Appl. Bio Mater. XXXX, XXX, XXX−XXX

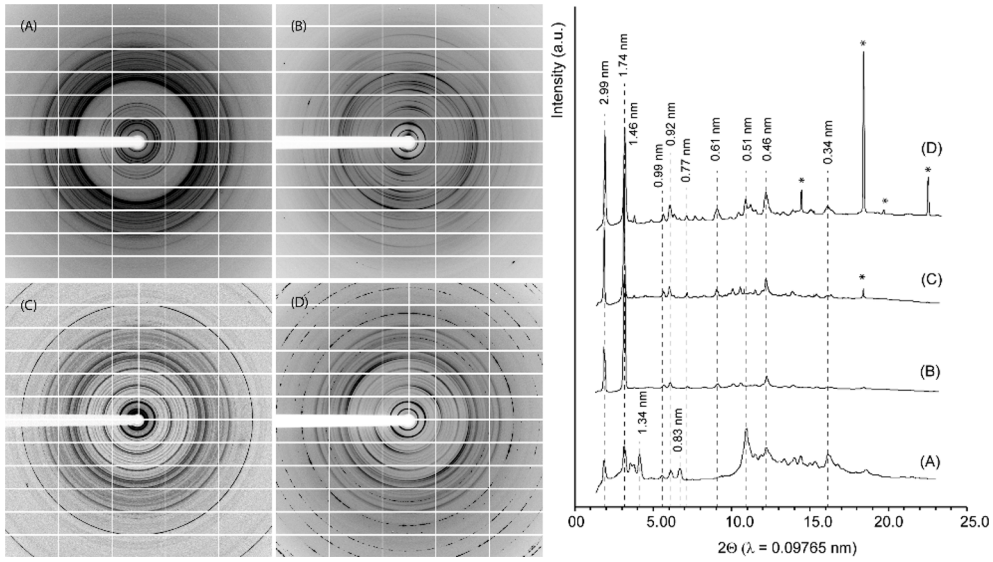

Figure 8. (left) Synchrotron X-ray fiber diffraction image of the samples **xero-1** (A), **xero-2** (B), **xero-3** (C), and **xero-4** (D). (right) Corresponding powder diffraction profiles obtained by integration of the intensities along the 2Θ angle. The main diffraction peaks from the xerogel structure are indicated with their associated periodicities. The diffraction peaks of calcite are marked by an asterisk (PDF: 01-086-0174).

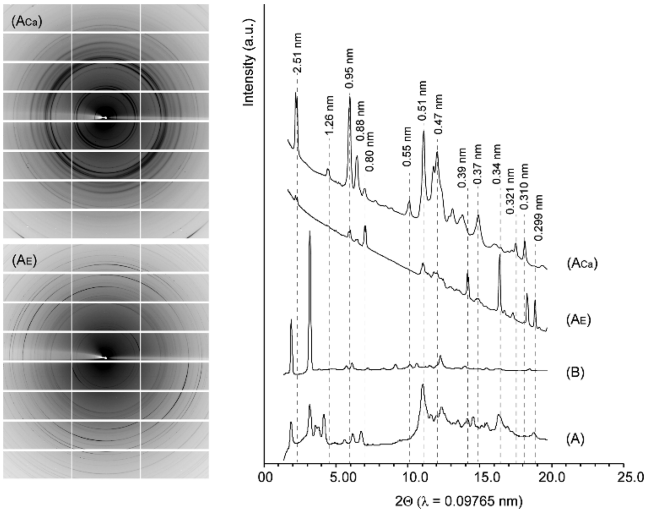

Figure 9. (left) Synchrotron X-ray fiber diffraction image of the samples **xero-2E** (A_E) and **xero-2Ca** (A_{Ca}). (right) Corresponding X-ray powder diffraction profiles obtained by integration of the intensities along the 2Θ angle. The main diffraction peaks from the xerogel structure are indicated with their associated periodicities. The X-ray powder diffraction profiles from the samples **xero-1** (A) and **xero-2** (B) are reported for comparison.

of Ca^{2+}, and **xero-2**, formed in the presence of Ca^{2+}, with the exception of diffraction peaks at 0.51 and 0.46 nm. In **xero-2E** or **xero-2Ca**, low-angle diffraction peaks were at 2.51 and 1.26 nm. In the same samples, other intense peaks were observed at 0.94, 0.87, and 0.37 nm, while in the sample **xero-2** most of these peaks were very weak.

Xerogels **xero-3#** and **xero-4#** show a different fiber organization and morphology and the presence of fiber bundles (Figure S10). These bundles gave X-ray diffraction fiber images (Figure S11) in which the meridional and equatorial direction could be identified. The analysis shows that the periodicities at 0.51 and 0.46 nm were along meridional, i.e., the fiber axis, while those at low diffraction angles, 2.21 and 1.74 nm, were along the equatorial axis.

In all analyzed samples, diffraction peaks which correspond to meridional periodicities at 0.51 and 0.46 nm, although with different relative intensities, were observed, while the periodicities of the respective low-angle diffraction peaks were different. This observation suggests that these periodicities (i.e., 0.51 and 0.46 nm) could be associated with the molecular packing along the fiber axis, as reported for tripeptides self-assembling in hydrogels.[70,71]

The periodicities along the equatorial axis (2.21 and 1.74 nm) seem to be more related to the content of the trigger, GdL or Ca^{2+}, within the crystalline fibers, which affects the molecular packing in the directions perpendicular to the fiber axis.

The calcified xerogel, **xero-3** and **xero-4**, showed addition diffraction peaks at about 0.38, 0.301, and 0.228 nm that correspond to diffraction peaks of calcite {01.2}, {10.4}, and {11.3}.[72] No diffraction peaks that could be associated to other anhydrous or hydrated calcium carbonate polymorphs were observed. The diffraction patterns did not show the presence of an intense background signal that could suggest the presence of relevant amounts of amorphous calcium carbonate. The relative intensity of the diffraction peaks of calcite with respect to those of the fibers was higher in the samples **xero-4** than in the samples **xero-3**, indicating a higher concetration (no quantified) of calcite in agreement with the higher concentration of Ca^{2+} and CO_3^{2-} in the starting hydrogel chemical system, as already observed from the SEM images.

In the above discussion, it is supposed that the structural organization of gelator fibers in the hydrogel is conserved, at least in part, in the xerogel. This could not be true; however, it was observed that the xerogels obtained after washing of the hydrogel were different from those obtained by only drying, suggesting a correlation between the xerogel and its parent hydrogel.

CONCLUSIONS

SAFiN hydrogels have a simple and robust preparation process that favors their potential application in different fields,[30−37] here as a bioinspired matrix for calcification. They formed

DOI: 10.1021/acsabm.9b00828
ACS Appl. Bio Mater. XXXX, XXX, XXX−XXX

through electrostatic and $\pi-\pi$ stacking interactions of Boc-L-DOPA$(OBn)_2$-OH molecules in aqueous alkaline conditions. The four kinds of hydrogels were prepared by varying the trigger (GdL or $CaCl_2$) and the base. They were solid-like with mechanical, compositional, and structural properties depending on the choice of the trigger. When Na_2CO_3 was used to alkalinize and $CaCl_2$ as a trigger, calcite crystals formed within the conserved solid-like hydrogel, generating a composite material. When Ca^{2+} was replaced with H^+, the SAFiN hydrogel assumed the same properties of the one formed using GdL as a trigger. This suggested that once assembled the hydrogel molecular chains relayed more on the $\pi-\pi$ stacking interactions than on the source of the electrostatic ones.

The calcified hydrogels produced xerogels that gave different X-ray fiber diffraction pattern and morphology if they were washed before the drying. It has been supposed that the interfibril interactions were affected by the washing that removed unreacted molecules and free ions, besides changing the chemical environment. Of course, these considerations are derivated by observations on xerogels and could not be representative of the fiber structures and interactions in the hydrogels.

In all xerogels from calcified hydrogels, calcite crystals were observed to be entrapped in the fiber network and entrapping fibers within their structure, generating a composite material. This scenario is supposed to be a realistic prediction of the hydrogel since calcite formed in the hydrogel. In addition, the amount of calcite crystals formed, which was qualitatively evaluated, increasing the concentrations of calcium and carbonate ions in the starting hydrogel chemical system. These final observations confirm the starting hypothesis that the fibrous structure of the hydrogel can be considered a bioinspired matrix that has the capability to confine the space of mineralization, to act as a source of Ca^{2+}, and to preserve its structural organization once the mineral formation has occurred, as frequently occurs in biomineralization.

■ ASSOCIATED CONTENT

Supporting Information

The Supporting Information is available free of charge at https://pubs.acs.org/doi/10.1021/acsabm.9b00828.

Preparation of the gelator Boc-L-DOPA$(OBn)_2$-OH; ^{1}H NMR, ^{13}C NMR, and LC-MS spectra of gelator **A**; amplitude sweep experiments on **1**, **2**, **3**, and **4**; photograph of a hydrogel **2** sample suspended into a 0.05 M EDTA solution; amplitude sweep experiments on **2E** compared with **2** and **1**; amplitude sweep and frequency sweep experiments on **2Ca** compared with **2E**; EDX analysis of the samples **xero-2E** and **xero-2Ca**; xerogel formed using a different procedure: samples **xero-3#** and **xero-4#**; SEM images of the xerogel samples **xero-3#** and **xero-4#**; and synchrotron X-ray fiber diffraction image of the samples **xero-3#** and **xero-4#** (PDF)

■ AUTHOR INFORMATION

Corresponding Authors

*E-mail: claudia.tomasini@unibo.it.

*E-mail: giuseppe.falini@unibo.it.

ORCID

Lara Jurković: 0000-0001-7229-9054

Damir Kralj: 0000-0002-4152-4893

Claudia Tomasini: 0000-0002-6310-2704

Funding

C.T. acknowledges the University of Bologna and Ministero dell'Università e della Ricerca (PRIN 2015 project 20157WW5EH). G.F. and S.F. thank Consorzio Interuniversitario di Ricerca sulla Chimica dei Metalli nei Sistemi Biologici for the support. L.S. and D.K. acknowledged the financial support by the Croatian Science Foundation (project IP-2013-11-5055).

Notes

The authors declare no competing financial interest.

■ ACKNOWLEDGMENTS

We thank the XRD1 beamline, Elettra, Trieste, Italy, and the ID23-1 beamline, ESRF, Grenoble, France, for the collection of the X-ray diffraction images.

■ REFERENCES

(1) Okesola, B. O.; Smith, D. K. Applying Low-Molecular Weight Supramolecular Gelators in an Environmental Setting – Self-Assembled Gels as Smart Materials for Pollutant Removal. *Chem. Soc. Rev.* **2016**, *45* (15), 4226–4251.

(2) Colquhoun, C.; Draper, E.; Schweins, R.; Marcello, M.; Serpell, L.; Vadukul, D.; Adams, D. Controlling the Network Type in Self-Assembled Dipeptide Hydrogels. *Soft Matter* **2017**, *13* (9), 1914–1919.

(3) Venkatesh, V.; Mishra, N. K.; Romero-Canelón, I.; Vernooij, R. R.; Shi, H.; Coverdale, J. P. C.; Habtemariam, A.; Verma, S.; Sadler, P. J. Supramolecular Photoactivatable Anticancer Hydrogels. *J. Am. Chem. Soc.* **2017**, *139* (16), 5656–5659.

(4) Ramin, M. A.; Latxague, L.; Sindhu, K. R.; Chassande, O.; Barthélémy, P. Low Molecular Weight Hydrogels Derived from Urea Based-Bolaamphiphiles as New Injectable Biomaterials. *Biomaterials* **2017**, *145*, 72–80.

(5) Huang, G.; Li, F.; Zhao, X.; Ma, Y.; Li, Y.; Lin, M.; Jin, G.; Lu, T. J.; Genin, G. M.; Xu, F. Functional and Biomimetic Materials for Engineering of the Three-Dimensional Cell Microenvironment. *Chem. Rev.* **2017**, 12764–12850, DOI: 10.1021/acs.chemrev.7b00094.

(6) Frith, W. J. Self-Assembly of Small Peptide Amphiphiles, the Structures Formed and Their Applications. (a Foods and Home and Personal Care Perspective). *Philos. Trans. R. Soc., A* **2016**, *374* (2072), 20150138.

(7) Nolan, M. C.; Fuentes Caparrós, A. M.; Dietrich, B.; Barrow, M.; Cross, E. R.; Bleuel, M.; King, S. M.; Adams, D. J. Optimising Low Molecular Weight Hydrogels for Automated 3D Printing. *Soft Matter* **2017**, *13* (45), 8426–8432.

(8) Sydney Gladman, A.; Matsumoto, E. A.; Nuzzo, R. G.; Mahadevan, L.; Lewis, J. A. Biomimetic 4D Printing. *Nat. Mater.* **2016**, *15* (4), 413–418.

(9) Ben Messaoud, G.; Le Griel, P.; Hermida-Merino, D.; Roelants, S. L. K. W.; Soetaert, W.; Stevens, C. V.; Baccile, N. PH-Controlled Self-Assembled Fibrillar Network (SAFiN) Hydrogels: Evidence of a Kinetic Control of the Mechanical Properties. *Chem. Mater.* **2019**, *31* (13), 4817.

(10) Ajay Mallia, V.; Weiss, R. G. Correlations between Thixotropic and Structural Properties of Molecular Gels with Crystalline Networks. *Soft Matter* **2016**, *12* (16), 3665–3676.

(11) Wang, X.; Liu, Z.; Ye, X.; Hu, K.; Zhong, H.; Yu, J.; Jin, M.; Guo, Z. A Facile One-Step Approach to Functionalized Graphene Oxide-Based Hydrogels Used as Effective Adsorbents toward Anionic Dyes. *Appl. Surf. Sci.* **2014**, *308*, 82–90.

(12) Du, X.; Zhou, J.; Shi, J.; Xu, B. Supramolecular Hydrogelators and Hydrogels: From Soft Matter to Molecular Biomaterials. *Chem. Rev.* **2015**, *115* (24), 13165–13307.

(13) Frith, W. J.; Donald, A. M.; Adams, D. J.; Aufderhorst-Roberts, A. Gels Formed from Amino-Acid Derivatives, Their Novel Rheology

DOI: 10.1021/acsabm.9b00828
ACS Appl. Bio Mater. XXXX, XXX, XXX–XXX

as Probed by Bulk and Particle Tracking Rheological Methods. *J. Non-Newtonian Fluid Mech.* **2015**, *222*, 104−111.
(14) Chakraborty, P.; Gazit, E. Amino Acid Based Self-Assembled Nanostructures: Complex Structures from Remarkably Simple Building Blocks. *ChemNanoMat* **2018**, *4* (8), 730−740.
(15) Jacob, R. S.; Ghosh, D.; Singh, P. K.; Basu, S. K.; Jha, N. N.; Das, S.; Sukul, P. K.; Patil, S.; Sathaye, S.; Kumar, A.; Chowdhury, A.; Malik, S.; Sen, S.; Maji, S. K. S. Self Healing Hydrogels Composed of Amyloid Nano Fibrils for Cell Culture and Stem Cell Differentiation. *Biomaterials* **2015**, *54*, 97−105.
(16) Zanna, N.; Merlettini, A.; Tomasini, C. Self-Healing Hydrogels Triggered by Amino Acids. *Org. Chem. Front.* **2016**, *3* (12), 1699−1704.
(17) Raeburn, J.; Cardoso, A. Z.; Adams, D. J. The Importance of the Self-Assembly Process to Control Mechanical Properties of Low Molecular Weight Hydrogels. *Chem. Soc. Rev.* **2013**, *42* (12), 5143−5156.
(18) Jung, J. H.; Rim, J. A.; Han, W. S.; Lee, S. J.; Lee, Y. J.; Cho, E. J.; Kim, J. S.; Ji, Q.; Shimizu, T. Hydrogel Behavior of a Sugar-Based Gelator by Introduction of an Unsaturated Moiety as a Hydrophobic Group. *Org. Biomol. Chem.* **2006**, *4* (10), 2033−2038.
(19) Greenfield, M. A.; Hoffman, J. R.; De La Cruz, M. O.; Stupp, S. I. Tunable Mechanics of Peptide Nanofiber Gels. *Langmuir* **2010**, *26* (5), 3641−3647.
(20) Clemente, M. J.; Fitremann, J.; Mauzac, M.; Serrano, J. L.; Oriol, L. Synthesis and Characterization of Maltose-Based Amphiphiles as Supramolecular Hydrogelators. *Langmuir* **2011**, *27* (24), 15236−15247.
(21) Jung, J. H.; John, G.; Masuda, M.; Yoshida, K.; Shinkai, S.; Shimizu, T. Self-Assembly of a Sugar-Based Gelator in Water: Its Remarkable Diversity in Gelation Ability and Aggregate Structure. *Langmuir* **2001**, *17* (23), 7229−7232.
(22) Brizard, A.; Oda, R.; Huc, I. Chirality Effects in Self-Assembled Fibrillar Networks. *Top. Curr. Chem.* **2005**, *256* (July), 167−218.
(23) Draper, E. R.; Adams, D. J. Low-Molecular-Weight Gels: The State of the Art. *Chem.* **2017**, *3* (3), 390−410.
(24) Podder, D.; Chowdhury, S. R.; Nandi, S. K.; Haldar, D. Tripeptide Based Super-Organogelators: Structure and Function. *New J. Chem.* **2019**, *43*, 3743−3749.
(25) Saha, A.; Bolisetty, S.; Handschin, S.; Mezzenga, R. Self-Assembly and Fibrillization of a Fmoc-Functionalized Polyphenolic Amino Acid. *Soft Matter* **2013**, *9* (43), 10239−10242.
(26) Qiao, Y.; Lin, Y.; Yang, Z.; Chen, H.; Zhang, S.; Yan, Y.; Huang, J. Unique Temperature-Dependent Supramolecular Self-Assembly: From Hierarchical 1D Nanostructures to Super Hydrogel. *J. Phys. Chem. B* **2010**, *114* (36), 11725−11730.
(27) Jayawarna, V.; Ali, M.; Jowitt, T. A.; Miller, A. F.; Saiani, A.; Gough, J. E.; Ulijn, R. V. Nanostructured Hydrogels for Three-Dimensional Cell Culture through Self-Assembly of Fluorenylmethoxycarbonyl-Dipeptides. *Adv. Mater.* **2006**, *18* (5), 611−614.
(28) Ozbas, B.; Kretsinger, J.; Rajagopal, K.; Schneider, J. P.; Pochan, D. J. Salt-Triggered Peptide Folding and Consequent Self-Assembly into Hydrogels with Tunable Modulus. *Macromolecules* **2004**, *37* (19), 7331−7337.
(29) Zanna, N.; Focaroli, S.; Merlettini, A.; Gentilucci, L.; Teti, G.; Falconi, M.; Tomasini, C. Thixotropic Peptide-Based Physical Hydrogels Applied to Three-Dimensional Cell Culture. *ACS Omega* **2017**, *2* (5), 2374−2381.
(30) Das, D.; Kar, T.; Das, P. K. Gel-Nanocomposites: Materials with Promising Applications. *Soft Matter* **2012**, *8* (8), 2348−2365.
(31) Iglesias, D.; Bosi, S.; Melchionna, M.; Da Ros, T.; Marchesan, S. The Glitter of Carbon Nanostructures in Hybrid/Composite Hydrogels for Medicinal Use. *Curr. Top. Med. Chem.* **2016**, *16* (18), 1976−1989.
(32) Zheng, H.; Neo, C. Y.; Mei, X.; Qiu, J.; Ouyang, J. Reduced Graphene Oxide Films Fabricated by Gel Coating and Their Application as Platinum-Free Counter Electrodes of Highly Efficient Iodide/Triiodide Dye-Sensitized Solar Cells. *J. Mater. Chem.* **2012**, *22* (29), 14465.
(33) Zhang, L. Y.; Wang, T.; Wang, H. Y.; Meng, Y.; Yu, W. T.; Chai, L. Y. Graphene@poly(m-Phenylenediamine) Hydrogel Fabricated by a Facile Post-Synthesis Assembly Strategy. *Chem. Commun.* **2013**, *49* (85), 9974−9976.
(34) Wang, H.; Han, A.; Cai, Y.; Xie, Y.; Zhou, H.; Long, J.; Yang, Z. Multifunctional Biohybrid Hydrogels for Cell Culture and Controlled Drug Release. *Chem. Commun. (Cambridge, U. K.)* **2013**, *49* (67), 7448−7450.
(35) Perale, G.; Giordano, C.; Bianco, F.; Rossi, F.; Tunesi, M.; Daniele, F.; Crivelli, F.; Matteoli, M.; Masi, M. Hydrogel for Cell Housing in the Brain and in the Spinal Cord. *Int. J. Artif. Organs* **2011**, *34* (3), 295−303.
(36) Weingarten, A. S.; Kazantsev, R. V.; Palmer, L. C.; Fairfield, D. J.; Koltonow, A. R.; Stupp, S. I. Supramolecular Packing Controls H2 Photocatalysis in Chromophore Amphiphile Hydrogels. *J. Am. Chem. Soc.* **2015**, *137* (48), 15241−15246.
(37) Schön, E.; Saldías, C.; Haldar, D.; Díaz, D. A Preliminary Comparative Study of the Baylis−Hillman Reaction in Ionic Liquid Solution and Gelled Ionic Liquid. *Macromol. Symp.* **2019**, *385* (1), 1800193.
(38) Weiner, S.; Addadi, L. Crystallization Pathways in Biomineralization. *Annu. Rev. Mater. Res.* **2011**, *41* (1), 21−40.
(39) Lowenstam, H. A.; Heinz, A.; Weiner, S. *On Biomineralization*; Oxford University Press, 1989.
(40) Van Driessche, A. E. S.; Kellermeier, M.; Benning, L. G.; Gebauer, D.*New Perspectives and Growth Nucleation on Mineral. From Solutions Precursors to Solid Materials*; 2017; Springer Nature: Springer Nature: Switzerland AG.
(41) Gómez-Morales, J.; Falini, G.; García-Ruiz, J. M. Biological Crystallization. In *Handbook of Crystal Growth*; Elsevier, 2015; Vol. *1*, pp 873−913. DOI: 10.1016/B978-0-444-56369-9.00020-4.
(42) Clark, A. H. Biopolymer Gels. *Curr. Opin. Colloid Interface Sci.* **1996**, *1* (6), 712−717.
(43) Godeau, G.; Barthélémy, P. Glycosyl-Nucleoside Lipids as Low-Molecular-Weight Gelators. *Langmuir* **2009**, *25* (15), 8447−8450.
(44) Sancho-Tomas, M.; Fermani, S.; Duran-Olivencia, M. A.; Otalora, F.; Gomez-Morales, J.; Falini, G.; Garcia-Ruiz, J. M. Influence of Charged Polypeptides on Nucleation and Growth of CaCO 3 Evaluated by Counterdiffusion Experiments. *Cryst. Growth Des.* **2013**, *13*, 3884.
(45) Asenath-Smith, E.; Li, H.; Keene, E. C.; Seh, Z. W.; Estroff, L. A. Crystal Growth of Calcium Carbonate in Hydrogels as a Model of Biomineralization. *Adv. Funct. Mater.* **2012**, *22* (14), 2891−2914.
(46) Kosanović, C.; Fermani, S.; Falini, G.; Kralj, D.; Kosanović, C.; Fermani, S.; Falini, G.; Kralj, D. Crystallization of Calcium Carbonate in Alginate and Xanthan Hydrogels. *Crystals* **2017**, *7* (12), 355.
(47) Mass, T.; Giuffre, A. J.; Sun, C.-Y.; Stifler, C. A.; Frazier, M. J.; Neder, M.; Tamura, N.; Stan, C. V.; Marcus, M. A.; Gilbert, P. U. P. A. Amorphous Calcium Carbonate Particles Form Coral Skeletons. *Proc. Natl. Acad. Sci. U. S. A.* **2017**, *114* (37), E7670−E7678.
(48) Magoulas, G. E.; Rigopoulos, A.; Piperigkou, Z.; Gialeli, C.; Karamanos, N. K.; Takis, P. G.; Troganis, A. N.; Chrissanthopoulos, A.; Maroulis, G.; Papaioannou, D. Synthesis and Antiproliferative Activity of Two Diastereomeric Lignan Amides Serving as Dimeric Caffeic Acid-l-DOPA Hybrids. *Bioorg. Chem.* **2016**, *66*, 132−144.
(49) Gaucher, A.; Dutot, L.; Barbeau, O.; Hamchaoui, W.; Wakselman, M.; Mazaleyrat, J. P. Synthesis of Terminally Protected (S)-B3-H-DOPA by Arndt-Eistert Homologation: An Approach to Crowned *β*-Peptides. *Tetrahedron: Asymmetry* **2005**, *16* (4), 857−864.
(50) Hammersley, A. P. FIT2D: A Multi-Purpose Data Reduction, Analysis and Visualization Program. *J. Appl. Crystallogr.* **2016**, *49* (2), 646−652.
(51) Zanna, N.; Merlettini, A.; Tatulli, G.; Milli, L.; Focarete, M. L. M. L.; Tomasini, C. Hydrogelation Induced by Fmoc-Protected Peptidomimetics. *Langmuir* **2015**, *31* (44), 12240−12250.
(52) Tomasini, C.; Zanna, N. Oxazolidinone-Containing Pseudopeptides: Supramolecular Materials, Fibers, Crystals, and Gels. *Biopolymers* **2017**, *108* (1), 1−14.

DOI: 10.1021/acsabm.9b00828
ACS Appl. Bio Mater. XXXX, XXX, XXX−XXX

(53) Zanna, N.; Iaculli, D.; Tomasini, C. The Effect of L-DOPA Hydroxyl Groups on the Formation of Supramolecular Hydrogels. *Org. Biomol. Chem.* **2017**, *15* (27), 5797−5804.
(54) Giuri, D.; Zanna, N.; Tomasini, C. Low Molecular Weight Gelators Based on Functionalized L-Dopa Promote Organogels Formation. *Gels* **2019**, *5* (2), 27.
(55) Zanna, N.; Focaroli, S.; Merlettini, A.; Gentilucci, L.; Teti, G.; Falconi, M.; Tomasini, C. Thixotropic Peptide-Based Physical Hydrogels Applied to Three-Dimensional Cell Culture. *ACS Omega* **2017**, *2* (5), 2374−2381.
(56) Chen, L.; McDonald, T. O.; Adams, D. J. Salt-Induced Hydrogels from Functionalised-Dipeptides. *RSC Adv.* **2013**, *3* (23), 8714.
(57) Chen, L.; Pont, G.; Morris, K.; Lotze, G.; Squires, A.; Serpell, L. C.; Adams, D. J. Salt-Induced Hydrogelation of Functionalised-Dipeptides at High PH. *Chem. Commun.* **2011**, *47* (44), 12071−12073.
(58) Mcewen, H.; Du, E. Y.; Mata, J. P.; Thordarson, P.; Martin, A. D. Tuning Hydrogels through Metal-Based Gelation Triggers. *J. Mater. Chem. B* **2017**, *5* (47), 9412−9417.
(59) Adams, D. J.; Butler, M. F.; Frith, W. J.; Kirkland, M.; Mullen, L.; Sanderson, P. A New Method for Maintaining Homogeneity during Liquid−Hydrogel Transitions Using Low Molecular Weight Hydrogelators. *Soft Matter* **2009**, *5* (9), 1856−1862.
(60) Yu, G.; Yan, X.; Han, C.; Huang, F. Characterization of Supramolecular Gels. *Chem. Soc. Rev.* **2013**, *42* (16), 6697−6722.
(61) Gong, Z.; Yang, Y.; Ren, Q.; Chen, X.; Shao, Z. Injectable Thixotropic Hydrogel Comprising Regenerated Silk Fibroin and Hydroxypropylcellulose. *Soft Matter* **2012**, *8* (10), 2875.
(62) Liu, Y.; Ling, S.; Wang, S.; Chen, X.; Shao, Z. Thixotropic Silk Nanofibril-Based Hydrogel with Extracellular Matrix-like Structure. *Biomater. Sci.* **2014**, *2* (10), 1338−1342.
(63) Pek, Y. S.; Wan, A. C. A.; Ying, J. Y. The Effect of Matrix Stiffness on Mesenchymal Stem Cell Differentiation in a 3D Thixotropic Gel. *Biomaterials* **2010**, *31* (3), 385−391.
(64) Li, Y.; Zhou, F.; Wen, Y.; Liu, K.; Chen, L.; Mao, Y.; Yang, S.; Yi, T. (−)-Menthol Based Thixotropic Hydrogel and Its Application as a Universal Antibacterial Carrier. *Soft Matter* **2014**, *10* (17), 3077−3085.
(65) Basak, S.; Nanda, J.; Banerjee, A. Multi-Stimuli Responsive Self-Healing Metallo-Hydrogels: Tuning of the Gel Recovery Property. *Chem. Commun.* **2014**, *50* (18), 2356−2359.
(66) Karan, C. K.; Bhattacharjee, M. Self-Healing and Moldable Metallogels as the Recyclable Materials for Selective Dye Adsorption and Separation. *ACS Appl. Mater. Interfaces* **2016**, *8* (8), 5526−5535.
(67) Roy, S.; Baral, A.; Banerjee, A. An Amino-Acid-Based Self-Healing Hydrogel: Modulation of the Self-Healing Properties by Incorporating Carbon-Based Nanomaterials. *Chem. - Eur. J.* **2013**, *19* (44), 14950−14957.
(68) Liu, Y.; Ling, S.; Wang, S.; Chen, X.; Shao, Z. Thixotropic Silk Nanofibril-Based Hydrogel with Extracellular Matrix-like Structure. *Biomater. Sci.* **2014**, *2* (10), 1338−1342.
(69) Yandell, B. S. *Practical Data Analysis for Designed Experiments*; Routledge, 2017. DOI: 10.1201/9780203742563.
(70) Janiak, C. A Critical Account on N-n Stacking in Metal Complexes with Aromatic Nitrogen-Containing Ligands. *J. Chem. Soc. Dalt. Trans.* **2000**, No. 21, 3885−3896.
(71) Cheng, G.; Castelletto, V.; Jones, R. R.; Connon, C. J.; Hamley, I. W. Hydrogelation of Self-Assembling RGD-Based Peptides. *Soft Matter* **2011**, *7*, 1326−1333.
(72) ICDD. PDF-4+ 2019 (Database); *Int. Cent. Diffr. Data*; Soorya, K., Ed.; Newt. Square: PA, USA, 2018.

DOI: 10.1021/acsabm.9b00828
ACS Appl. Bio Mater. XXXX, XXX, XXX−XXX